Quantitative PET/CT imaging and dosimetry of 89Zr labelled compounds

Makris, N.

2015

document version
Publisher's PDF, also known as Version of record

6

An automatic delineation method for bone marrow absorbed dose estimation in ^{89}Zr PET/CT studies

Nikolaos E. Makris, Ronald Boellaard, Catharina W. Menke,
Adriaan A. Lammertsma and Marc C. Huisman

Nikolaos E. Makris, Ronald Boellaard, Catharina W. Menke, Adriaan A. Lammertsma and Marc C. Huisman. An automatic delineation method for bone marrow absorbed dose estimation in ^{89}Zr PET/CT studies. Submitted in EJNMMI physics

Abstract

To develop and validate an (active contour based) automatic delineation method for estimating red marrow (RM) activity concentration and absorbed dose in ^{89}Zr Positron emission tomography/computed tomography (PET/CT) studies.

Methods: Five patients with advanced colorectal cancer were received 37.1 ± 0.9 MBq ^{89}Zr-cetuximab within 2 hours after administration of a therapeutic dose of 500 mg·m^{-2} unlabelled cetuximab. Per patient, five PET/CT scans were acquired on a Gemini TF-64 PET/CT scanner at 1, 24, 48, 96 and 144 h post injection, respectively. Low dose CT data were used to manually generate volumes of interest (VOI) in the lumbar vertebrae (LV). In addition, LV VOI were generated automatically using an active contour method in a low dose CT. RM activity was then determined by mapping the low dose CT derived RM VOI onto the corresponding PET scans. Finally, these activities were used to derive residence times and, subsequently, the self and total RM absorbed doses using OLINDA/EXM 1.1.

Results: High correlations ($r^2 = 0.85$) between manual and automated VOI methods were obtained for both RM activity concentrations and total absorbed doses. On average, the automatic method provided values that were lower by 5% compared to the manual method.

Conclusions: An automated and efficient VOI method was developed, enabling accurate estimates of RM activity concentrations and total absorbed doses.

6.1 Introduction

In radio-immunotherapy studies, red marrow (RM) often is the dose-limiting organ (1). RM is a complex and dynamic organ, which is distributed in different sites throughout the human body with the axial skeleton (i.e. vertebrae) being the main site. Positron emission tomography/computed tomography (PET/CT) allows for assessment of RM radioactivity concentrations as function of time and for estimation of absorbed radiation doses. Conventionally, the plasma time-activity curve is multiplied by a fixed factor (e.g. 0.19) to estimate the RM time-activity curve (2). However, there is increasing evidence that the use of a fixed factor may be inaccurate, because the red marrow to plasma activity concentration ratio is not constant and increases over time (3–5). Consequently, a plasma based approach could lead to underestimation of RM absorbed dose. Recent findings (6) showed that the use of standard peripheral blood sampling method may underestimate radiation absorbed dose to red marrow in patients undergoing ^{131}I-rituxumab radioimmunotherapy. Therefore, an image based method should be investigated as an alternative to the blood (or plasma) based methods.

In order to derive RM activity or dose estimates, a manual RM volume of interest method (VOI_{RM}), either defined directly onto the PET image or in a coregistered CT image, is used frequently, as it is simple and straightforward. However, it is also time consuming and labour intensive, especially when analysing several scans per patient. Therefore, an automatic VOI_{RM} method would be advantageous, as it may be both time efficient and observer independent. Such a method could be based on the use of a single Hounsfield unit (HU) threshold value applied to the CT image, allowing for bone marrow activity estimation from the coregistered PET image. However, it is well known that the lumbar vertebrae (LV) consists of different components (compact bone, red and yellow marrow, extracellular matrix), displaying a large range of HUs. Consequently, applying a threshold to the CT image may not be optimal, as it would not solely extract the red marrow component of the LV. This limitation might be overcome by using a more sophisticated active contour method (7) that first identifies the outer bone structure of the LV based on local intensity information in a low dose CT (ldCT) and subsequently partitions the LV between compact bone and bone marrow. The purpose of the present study was to develop such an active contour method and to validate it against results obtained from manual delineation.

6.2 Materials and methods

6.2.1 Imaging protocol

Five patients with advanced colorectal cancer were included. Patients received 37.1 ± 0.9 MBq ^{89}Zr-cetuximab within 2 h after administration of a therapeutic dose of 500 mg·m^{-2} unlabelled cetuximab. Per patient, five PET/CT scans were acquired on a Gemini TF-64 PET/CT scanner (Philips Healthcare, Cleveland, OH, USA) at 1, 24, 48, 96 and 144 h post injection, respectively. PET data were normalized, corrected for decay, randoms, dead time, scatter and attenuation, and reconstructed using a time-of-flight list-mode ordered-subsets expectation maximization reconstruction algorithm using an image matrix size of 144 × 144 and a voxel size of 4 × 4 × 4 mm^3.

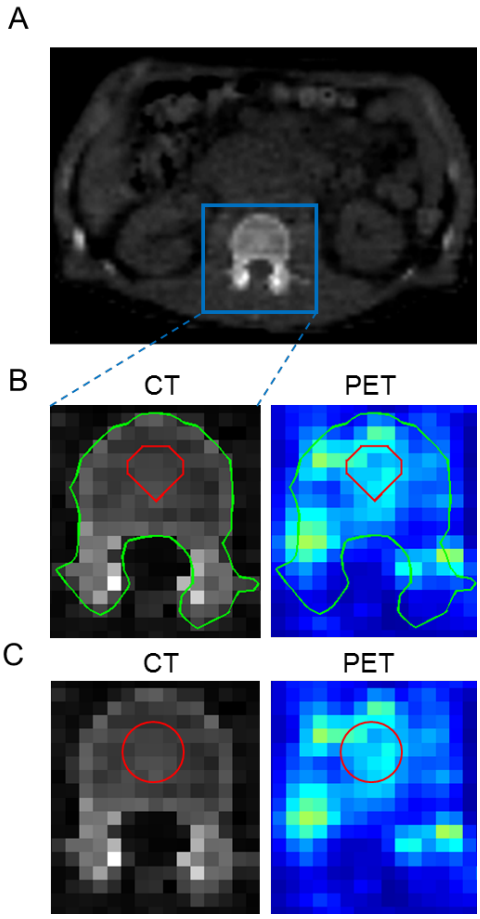

Figure 6.1. *Use of a low dose CT image (A) to derive active (B) and manual (C) contours in one CT slice which are then projected onto the coregistered PET image to determine radioactivity concentration of the enclosed volumes of interest. In each CT slice a loose region (c_1 - blue), enclosing the LV segment, was defined as the starting point of the active contour algorithm. In the next step, the active contour method was applied so as to identify the outer bone contour (c_2 - green) of the LV. Lastly, erosion of c_2 was performed by sampling three pixels (vertically and horizontally) so as to exclude the compact bone from the LV segment, allowing for the creation of a contour that encompasses only the bone marrow component (c_3 - red).*

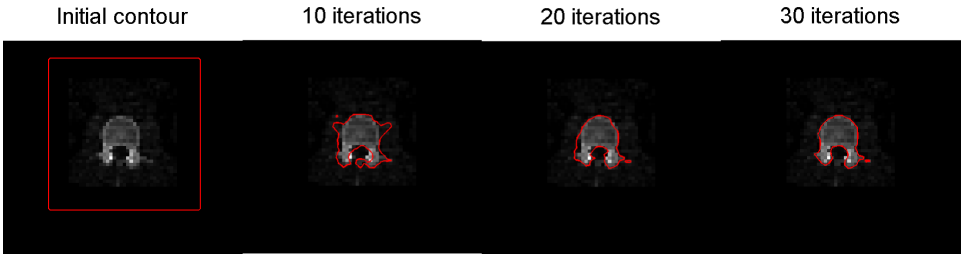

Figure 6.2. *Example of the contour evolution process from initial to final contour, depicting the detection of the outer bone contour of lumbar vertebrae in a single CT slice.*

In addition, for each time point, a 50 mAs ldCT scan was acquired for attenuation correction purposes. The corresponding ldCT images were reconstructed using an image matrix size of 512 × 512 and a voxel size of 1.17 × 1.17 × 5.00 mm^3. The study was approved by the Medical Ethics Review Committee of the VU University Medical Centre and informed consent was obtained from each patient prior to inclusion in the study.

6.2.2 Delineation methods

Manual delineation

Low dose CT scans were first rebinned (using software developed in-house) using trilinear interpolation with a 4 × 4 × 4 mm^3 voxel size in order to match matrix and voxel size of the PET images (Figure 6.1A). Volumes of interest (VOI) in bone marrow of the LV were drawn independently (Figure 6.1C) on all five ldCT scans of each patient. Subsequently, RM activity was determined by mapping the ldCT derived manual VOI_{RM} onto the corresponding PET scan.

Automatic delineation (active contour)

In a first initialization step, a region within a margin of about 1 cm was drawn around the five LV segments on the rebinned ldCT image (Figure 6.1A). Next, this manual VOI was used to produce an LV binary mask that was applied to the ldCT image for extracting a coarse CT region that contained the LV component (CT_1). The active contour model (see Appendix) used in this study is based on a work by Chen and Vese (7) which was later improved by enabling segmentation of images with weak object boundaries (8). Recently, the latter methodology was used by Sambuceti et al. (9) on CT data for extracting whole bone marrow volume. The active contour model was developed in MATLAB (Mathworks) environment and

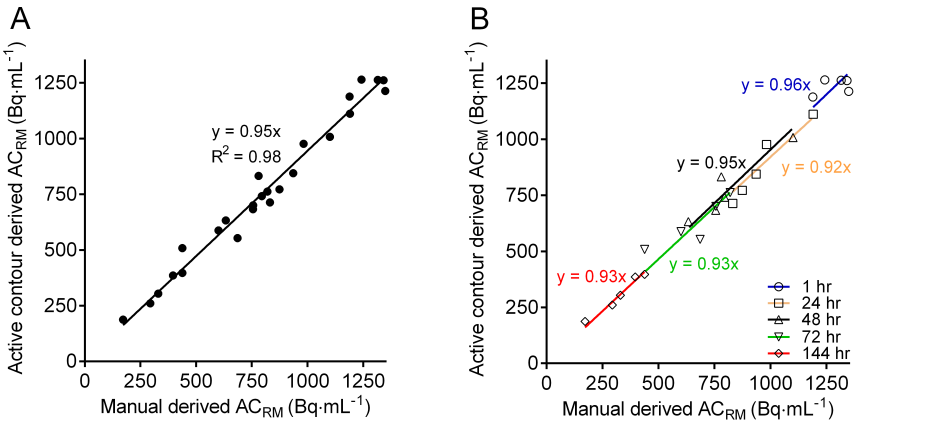

Figure 6.3. *Correlation between manual and automatic derived red marrow activity concentrations (Bq·mL^{-1}) for all patients (A) and per time point across all patients (B). The intercept was set to (0, 0).*

was applied to CT_1, where the LV bone contour (enclosing compact bone and bone marrow) was identified, providing a CT image of the compact bone and bone marrow (CT_2). This LV bone contour was eroded to exclude compact bone, thus, a three-pixel layer was removed from the outer bone contour, resulting in a CT image containing only the intraosseous volume (CT_3). Outer LV bone and intraosseous contours can be seen in (Figure 6.1B).

6.2.3 Organ dosimetry

After determining the mean activity concentration in a VOI_{RM} at all five time points, RM time-activity curves were generated. Other organs were delineated semi-automatically to derive organ time-activity curves (10). Cumulated activities were calculated as areas under the curves of RM and organ time-activity data by using the trapezoidal rule and assuming physical decay after the last measurement. The residence time in the remainder of the body was calculated as the maximum possible residence time assuming physical decay only (no biological clearance) minus the sum of residence time of source organs. The organ residence times were scaled according to patient specific weight. Dose conversion factors (S-values) were taken from OLINDA/EXM 1.1 software and were used for calculation of organ and RM absorbed doses (11). Red marrow residence time data based on the plasma method were taken from Makris et al. (4), and the $S_{RM \leftarrow RM}$, $S_{RM \leftarrow RB}$, and

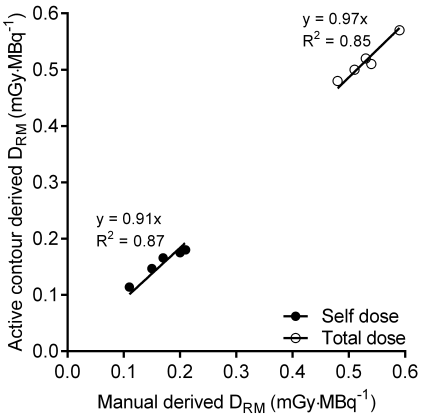

Figure 6.4. *Red marrow (RM) dose estimates based on manual and automatic delineation approaches for self (closed circles) and total dose (open circles).*

reference man/woman RM volume values used in the calculation of RM (self and total) absorbed dose were taken from OLINDA/EXM 1.1. $S_{RM \leftarrow RM}$ corresponds to the 'red marrow to red marrow' contribution and $S_{RM \leftarrow RB}$ corresponds to the 'remainder of the body to red marrow' contribution. As this study focused on RM, only RM self and total (including contributions from source organs) absorbed doses will be reported.

6.3 Results

Figure 6.2 shows a typical example of LV contour detection using an iterative optimization scheme in a CT slice. The number of iterations was thirty, as proposed by Li et al. (12).High correlations between manually and automatically derived RM activity concentration estimates were obtained, as shown in Figure 6.3A for all patients and time-points, and in Figure 6.3B per time point across all patients. The automatic method showed a slightly lower (5%) RM activity concentrations compared with the manual method. For both self and total RM absorbed doses, correlations between the two methods were higher than 0.85 (see Figure 6.4). Use of the automatic method resulted in self and total absorbed doses that were on average 8% and 3% lower, respectively, as compared with the manual method. Table 6.1summarizes RM (self and total) absorbed dose estimates for manual, automatic and plasma based approaches. Significant differences ($p<0.05$) were seen between both image based approaches and the plasma based method in estimating RM self absorbed dose.

Table 6.1. *RM absorbed dose.*

	RM self dose mGy·MBq^{-1}	RM total dose mGy·MBq^{-1}
Manual delineation	0.17 ± 0.04	0.51 ± 0.04
Active contour	0.16 ± 0.03	0.49 ± 0.03
Plasma method	0.11 ± 0.03	0.45 ± 0.04

6.4 Discussion

Automatically derived RM activity concentration were within 5% of manual derived estimates, indicating that the active contour method can identify the intraosseous activity concentration in the LV sufficiently accurately. As a result, accurate estimation of RM absorbed doses could be achieved, showing only a small discrepancy of about 3% in total dose compared with the manual method. In radio-immunotherapy, where pure or nearly pure β emitters are used, only the self RM absorbed dose component contributes to the total RM dose whereas in immunoPET both the self (electrons) and cross (photons) RM absorbed dose contribute to the total RM absorbed dose. Bone marrow biopsies have been used as the gold standard for assessing radioactivity concentration in the RM. Other procedures, however, that allow assessment of RM activity concentration based on the blood sampling or the PET image have been preferred due to their minimal or non invasive nature. Yet, several studies reported that a plasma based approach may not be reliable for accurately estimating RM absorbed doses, as it assumes a fixed RMPR over time (3–5). To be more specific, in our previous work it was found that a plasma based approach can underestimate RM absorbed dose by 40% (immunoPET setup) and 20% (radio-immunotherapy setup) when compared with an image based method (4). In addition, the use of manual based VOI$_{RM}$ showed that the RMPR increases as function of time. Consequently, image based methods for estimation of RM absorbed doses may be preferred. However, manual delineation of VOI$_{RM}$ is time consuming, making the development of an automated tool highly desirable. The present study showed that automatic VOI$_{RM}$ based RM doses were comparable to those obtained from manual VOI$_{RM}$ and thus allows for accurate image based RM dose estimates. As expected, plasma based RM absorbed doses deviated significantly from both image based RM absorbed doses. There are, however, some practical issues and limitations regarding the use of the present automated method. First, there is a pre-processing step in which the user needs to (roughly) extract the LV associated part of

the CT image. Secondly, in a small proportion (15%) of the automatically generated VOI_{RM}, minimal manual adjustments were needed in order to remove voxels (from the lower part of LV segments) that did not represent RM volume. Finally, it was assumed that ^{89}Zr activity was distributed homogeneously throughout the intraosseous volume (red and yellow marrow) of the LV. However, yellow marrow (adipose tissue), a non hematopoietically active tissue, is considered to be a marrow component with reduced activity concentration compared to red marrow. Additionally, the distribution of the different BM types is dependent upon the skeletal part analyzed, red marrow in the LV is substantially higher, i.e. 90% vs 10% of the intraosseous volume respectively (9, 13). Whereas, bones in the appendicular part of the skeleton is mainly occupied by yellow marrow. Consequently, the assumption of homogeneously distributed Zr activity in the intraosseous volume of the LV would minimally affect the RM activity concentration estimation, thus, with no notable implications for the conclusions of this study.

6.5 Conclusion

A time-efficient method with no or almost non observer interaction, for estimation of red marrow activity concentration in the lumbar vertebrae was developed. The method is based on an active contour approach, providing accurate estimates of red marrow total absorbed doses.

Appendix

An energy functional is defined in terms of a contour and two fitting functions that approximate the image intensities inside and outside the contour. The energy is then used into a variational level set formulation (ϕ: level set function) with a arc length term (a) which is used for maintaining the regularity of the contour and a level set regularization term (b) that serves in maintaining the regularity of the level set function. Subsequently, a curve evolution equation is derived so as to minimize the associated energy functional. Intensity information in local regions at a certain scale is used to compute the two fitting functions ($f_1(x)$ and $f_2(x)$) and thereby progressively adapt the contour toward the LV bone boundaries. The energy criterion is as follows:

$$E(\phi) = \lambda_1 \int_\Omega K_\sigma e_1(x) H(\phi(x)) dx + \lambda_2 \int_\Omega K_\sigma e_2(x)(1 - H(\phi(x))) dx + \nu \int_\Omega \delta(\phi(x)) \|\nabla\phi(x)\| dx + \mu \int_\Omega \frac{1}{2}(\|\nabla\phi(x)\| - 1)^2 dx \quad (6.1)$$

where $\delta(\phi)$ is the Dirac function, e_1 and e_2 are given by the following formula:

$$e_i(x) = \int |I(x) - f_i(x)|^2 dy, i = 1, 2 \quad (6.2)$$

and K_σ is a gaussian kernel defined as:

$$K_\sigma(u) = \frac{1}{(2\pi)^{n/2}\sigma^n} e^{\|u\|^2/2\sigma^2} \quad (6.3)$$

$f_1(x)$ and $f_2(x)$ approximate image intensities outside and inside the active contour and are given by the following equations:

$$f_1(x) = \frac{H_1(\phi(x))I(x)}{H_1(\phi(x))}, f_2(x) = \frac{(1 - H_2(\phi(x)))I(x)}{(1 - H_2(\phi(x)))} \quad (6.4)$$

$I(x)$ are the intensities used for the fitting energy, and *H(ϕ)* is a regularised version of the Heaviside function:

$$H(x) = \frac{1}{2}\left(1 + \frac{2}{\pi}\arctan\left(\frac{x}{\epsilon}\right)\right) \quad (6.5)$$

Minimization of the energy functional can be obtained by solving the evolution problem:

$$\frac{\partial\phi}{\partial t} = -\delta(\phi)(e_1 - e_2) + \underbrace{\delta(\phi) div\left(\frac{\nabla\phi}{|\nabla\phi|}\right)}_{a} + \underbrace{\left(\nabla^2\phi - div\left(\frac{\nabla\phi}{|\nabla\phi|}\right)\right)}_{b} \quad (6.6)$$

References

[1] K.S. Loke, A.K. Padhy, D.C. Ng, A.S. Goh, and C. Divgi. Dosimetric considerations in radioimmunotherapy and systemic radionuclide therapies: a review. *World J Nucl Med*, 10:122–138, 2011.

[2] G. Sgouros. Bone marrow dosimetry for radioimmunotherapy: theoretical considerations. *J Nucl Med*, 34:689–694, 1993.

[3] C. Hindorf, O. Linden, J. Tennvall, K. Wingardh, and S.E. Strand. Time dependence of the activity concentration ratio of red marrow to blood and implications for red marrow dosimetry. *Cancer*, 94(4 Suppl):1235–1239, 2002.

[4] N. Makris, R. Boellaard, A. van Lingen, A.A. Lammertsma, G. van Dongen, H. Verheul, C. Menke, and M. Huisman. Pet/ct derived whole body and bone marrow dosimetry of 89zr-cetuximab. *J Nucl Med*, 56:249–254, 2015.

[5] J. Schwartz, J.L. Humm, C.R. Divgi, S.M. Larson, and J.A. O'Donoghue. Bone marrow dosimetry using 124i-pet. *J Nucl Med*, 53:615–621, 2012.

[6] J.A. Boucek and J.H. Turner. Personalized dosimetry of 131i-rituximab radioimmunotherapy of non-hodgkin lymphoma defined by pharmacokinetics in bone marrow and blood. *Cancer Biother Radiopharm*, 29:18–25, 2014.

[7] T.F. Chan and L.A. Vese. Active contours without edges. *IEEE Trans Image Process*, 10:266–277, 2001.

[8] C. Li, C.Y. Kao, J.C. Gore, and Z. Ding. Minimization of region-scalable fitting energy for image segmentation. *IEEE Trans Image Process*, 17:1940–1949, 2008.

[9] G. Sambuceti, M. Brignone, C. Marini, M. Massollo, F. Fiz, S. Morbelli, A. Buschiazzo, C. Campi, R. Piva, A.M. Massone, M. Piana, and F. Frassoni. Estimating the whole bone-marrow asset in humans by a computational approach to integrated pet/ct imaging. *Eur J Nucl Med Mol Imaging*, 39:1326–1338, 2012.

[10] N.E. Makris, R. Boellaard, C.W. Menke A.A. Lammertsma, and M.C. Huisman. Validation of simplified dosimetry approaches in 89zr-pet/ct: The use of manual versus semi-automatic delineation methods to estimate organ absorbed doses. *Med Phys*, 41:102503, 2014.

[11] M.G. Stabin, R.B. Sparks, and E. Crowe. Olinda/exm: the second-generation personal computer software for internal dose assessment in nuclear medicine. *J Nucl Med*, 46:1023–1027, 2005.

[12] C. Li, C. Xu, C. Gui, and M.D. Fox. Distance regularized level set evolution and its application to image segmentation. *IEEE Trans Image Process*, 19:3243–3254, 2010.

[13] S. Basu, M. Houseni, G. Bural, W. Chamroonat, J. Udupa, S. Mishra, and A. Alavi. Magnetic resonance imaging based bone marrow segmentation for quantitative calculation of pure red marrow metabolism using 2-deoxy-2-[f-18]fluoro-d-glucose-positron emission tomography: a novel application with significant implications for combined structure-function approach. *Mol Imaging Biol*, 9:361–365, 2007.